CHEMISTRY OF MATERIALS

Article

pubs.acs.org/cm

Crystal Structure, Physical Properties, and Electrochemistry of Copper Substituted $LiFePO_4$ Single Crystals

Shailesh Upreti,[†,▲] Natasha A. Chernova,[†] Jie Xiao,[†,⊗] Joel K. Miller,[†,▼] Olga V. Yakubovich,[‡] Jordi Cabana,[§,○] Clare P. Grey,[§,#] Vincent L. Chevrier,[⊥,▽] Gerbrand Ceder,[⊥] Janice L. Musfeldt,[∥] and M. Stanley Whittingham*[,†]

[†]Chemistry and Materials, Binghamton University, Binghamton 13902, New York, United States

[‡]Department of Geology, Moscow State University, Moscow 119991, Russia

[§]Department of Chemistry, Stony Brook University, Stony Brook 11794, New York, United States

[⊥]Department of Materials Science and Engineering, Massachusetts Institute of Technology, Cambridge, Massachusetts 02139, United States

[∥]Department of Chemistry, University of Tennessee, Knoxville, Tennessee 37996, United States

ABSTRACT: Copper substituted lithium iron phosphate, with the olivine structure, has been synthesized hydrothermally as dark-brown single crystals with 15% of the iron sites occupied by cupric ions. Single crystal X-ray diffraction and magnetic susceptibility, combined with Li solid state NMR studies performed on powder sample, showed that 5% of the lithium ions also reside on the iron site, giving the formula $Li_{0.95}[(Fe^{2+})_{0.70}(Fe^{3+})_{0.10}(Cu^{2+})_{0.15}Li_{0.05})]PO_4$. The compound exhibits anisotropic magnetic susceptibility and orders antiferromagnetically at 48 K. The magnetic moments are aligned along [010] as in $LiFePO_4$. The optical measurements indicate that the dark brown color originates from interionic d-d transitions. A part of the lithium ions can be cycled in an electrochemical cell, corresponding to the oxidation/reduction of the iron ions. An onset of a second electrochemical process is observed at about 4.1 V, tentatively attributed to the removal of Li ions from the Fe site. The first principles calculations indicate above 5 V redox potential for the Cu^{2+}/Cu^{3+} pair in the olivine structure, much higher than experimentally observed. The diffusion coefficient is determined from galvanostatic intermittent titration data, as part of the delithiation process proceeds as a single-phase reaction in this disordered compound.

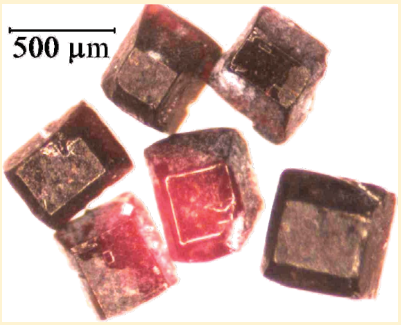

KEYWORDS: *copper olivine, hydrothermal synthesis, redox behavior*

INTRODUCTION

There has been much interest in understanding the chemical and physical behavior of the olivine class of materials typified by $LiFePO_4$, since the discovery by Padhi et al[1] of the ready and reversible intercalation of lithium in the crystalline lattice. Lithium ions diffuse along one-dimensional tunnels in the structure, so it is critical that the iron atoms and lithium atoms are perfectly ordered, so that lithium diffusion is not hindered.[2,3] The exact mechanism of the lithium insertion and removal in this two-phase $LiFePO_4/FePO_4$ system is still not fully understood. In very small crystallites, less than 20 nm, it is likely that a single phase may exist over much of the composition range, Li_xFePO_4,[4,5] so that lithium diffusion is rate-determining. In large crystallites, say 100 nm or larger, where the two phases are present, is the nucleation of the new phase rate-determining, or is it the diffusion of the charged species, lithium or electrons? Substituting a part of the iron by magnesium[6] or vanadium[7] enhances the capacity and rate capability. Such substitution is likely to reduce the perfect nature of the lattice and therefore reduce the nucleation energy for formation of the new phase.[7] In addition, this substitution leads to a denser nanostructure thereby increasing the tap density and reducing the amount of carbon needed for a conductive carbon coating. Substitution of a little iron for manganese in $LiMnPO_4$ is also reported to enhance its cyclability.[8]

$LiFePO_4$ and $LiMnPO_4$ are electronic insulators; there is a controversial report in the literature on the partial aliovalent substitution in the $LiFePO_4$ leading to enhanced electrical conductivity.[9] If partial substitution can enhance both the electronic conductivity of $LiFePO_4$ and its phase conversion, it is important that a better understanding of isovalent and aliovalent substitution be obtained. If trivalent ions can be substituted for iron or manganese in $Li(Fe, Mn)PO_4$, then vacancies should be generated on the lithium site, perhaps enhancing the lithium diffusivity.

To better understand the lithium deintercalation behavior and physical properties of the $LiFePO_4$ olivine, we set-out to form single crystals of a sufficient size to allow for their physical characterization. The hydrothermal method was chosen so that lower temperatures could be used than the 700 °C commonly used for solid state syntheses, where defective surface films such

Received: September 6, 2011
Revised: November 22, 2011
Published: November 22, 2011

   dx.doi.org/10.1021/cm2026619 | *Chem. Mater.* 2012, 24, 166–173

as iron phosphide might be formed.[10,11] Our previous hydrothermal work[2,3,12,13] showed that Fe/Li disorder can occur at temperatures lower than 200 °C. Thus, we chose conditions, 400 °C and 1000 atm, more typical of geological reactions. The reactions were performed in copper vessels, and the products formed contained up to 15% copper substitution on the iron site. In this paper we describe the synthesis and properties of one of the three copper containing compounds formed; the structure of the other one was reported separately,[14] while the third type of crystals did not produce solvable diffraction data.

EXPERIMENTAL SECTION

Single crystals were grown under high-temperature high-pressure hydrothermal conditions in the LiH_2PO_4–Fe_2O_3–H_3PO_4 system. Fe_2O_3 and LiH_2PO_4, molar ratio 3.25:1, were placed in an 8 mL copper ampule with 5, 10, 20, 30, or 40% water solution of H_3PO_4 filling 0.7 of the volume. The reaction was conducted at 400 °C and 1000 atm. for 100 h. A Jeol 8900 Electron Microprobe was used for the EDS elemental analysis. The single crystal X-ray diffraction data were collected at 298 K on a Bruker Smart 1000 diffractometer equipped with a CCD area detector using a graphite monochromator and a MoK_α radiation (λ = 0.71073 Å). A total of 3660 frames were collected with a scan width of 0.5° in ω and an exposure time of 15 s/frame using SMART software.[15] The frames were integrated using SAINT, measured intensities were reduced to F^2 and corrected for absorption with SADABS.[16] Structure solution, refinement, and data output were carried out with the SHELXTL program.[17] The bulk purity of manually separated single crystals was confirmed by powder X-ray diffraction on a Scintag XDS2000 diffractometer equipped with a Ge(Li) solid state detector and CuK_α radiation.

^{6}Li magic angle spinning nuclear magnetic resonance (MAS NMR) experiments were performed on a powder sample with a double-resonance 1.8 mm probe, built by A. Samoson and co-workers (KBFI, Tallinn, Estonia), on a CMX-200 spectrometer using a magnetic field of 4.7 T, at a spinning frequency of 38 kHz and using a Hahn-echo sequence with a 4.5 μs pulse width and an acquisition delay of 0.2 s. 1 M LiCl (at 0 ppm) was used as an external reference.

A large single crystal 400 × 300 × 100 μm in size was chosen for magnetic and optical properties studies (Figure 1). The magnetic properties were studied using a Quantum Design MPMS XL SQUID magnetometer. The single crystal was fixed in a plastic straw using a small amount of vacuum grease and temperature dependence of magnetization was measured from 298 to 2 K in a magnetic field of 1000 Oe directed along either *a*, *b*, or *c* crystallographic axes of the crystal.

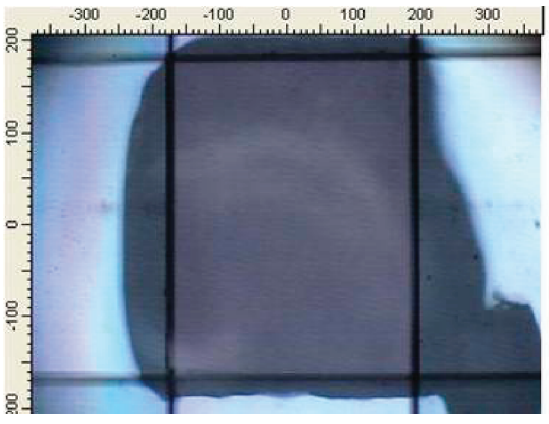

Figure 1. *bc*-plane image of indexed *o*-LiFeCuPhosphate single crystal used for the magnetic and optical property measurements. The 300 × 400 μm^2 sample is shown under the optical microscope along with the knife edge aperture positioned to show the measured sample.

The optical properties work was carried out on a series of instruments including a Bruker 113v Fourier transform infrared spectrometer with bolometer detector, an Equinox 55 spectrometer equipped with microscope attachment, and a Perkin-Elmer Lambda-900 grating spectrometer, covering the range from ~30–60,000 cm^{-1} (~3.7 meV–7.44 eV). Experiments were performed in both transmittance and reflectance mode, and absorption was calculated either as $\alpha(\omega) = -(1/hd)\ \ln(T(\omega))$, where h is the loading, d is the thickness, and $T(\omega)$ is the measured transmittance, or via a Kramers–Kronig analysis to obtain the optical constants.[18] Both a *bc*-plane-oriented single crystal and an isotropic pressed pellet were employed for these experiments.

The cathode electrode was prepared by hand grinding the single crystals, Teflon powder, and acetylene black in a weight ratio of 75:10:15. This mixture was hot-pressed into a stainless steel exmet grid, which was inserted into coin cells in a helium glovebox. Lithium foil was used as the anode and reference electrode, and the electrolyte was a 1 M solution of lithium hexafluorophosphate in a 1:1 volumetric mixture of dimethyl carbonate (DMC) and ethylene carbonate (EC). The loading of the active material was 9.96 mg per 0.33 cm^2 cathode; the cells were cycled between 2.0 and 4.5 V with a current density of 0.1 mA cm^{-2}. For the galvanostatic intermittent titration technique (GITT) measurements the material loading was 4.87 mg per 0.35 cm^2 cathode. A current of 0.08 mA was passed for $1^1/_4$ h, and the cell allowed to relax for 7 h, before the next current pulse was applied. A Bio-Logic VMP2 multichannel potentiostat was used to collect the electrochemical data.

Density functional theory (DFT) total energy calculations employing the HSE06 hybrid functional[19−21] were performed with the Vienna Ab-initio Simulation Package (VASP 5.2.2). Calculations were performed using the primitive cell of $LiFePO_4$ in the *Pnma* space group with Cu substituted for Fe when necessary, a 500 eV energy cutoff, and a 2 × 4 × 6 Monkhorst–Pack *k*-point mesh. Structural relaxations were performed to a tolerance of 2 × 10^{-4} eV/atom in the total energy and Fe and Cu atoms were initialized in ferromagnetic (FM) and antiferromagnetic (AFM) orderings. Standard methods were used to calculate the average Li intercalation potential.[22]

RESULTS AND DISCUSSION

The reaction product from the hydrothermal synthesis consisted of a mixture of brown, grayish-green, and blue-green crystals, white powder and copper chunks in a ratio dependent upon the phosphoric acid concentration. The crystals were hand-picked under an optical microscope, washed with water and isopropyl alcohol, dried and subjected to single-crystal X-ray diffraction and elemental analysis. All the copper found in the crystals could only have come from the copper reaction vessel used. The olivine structure was found for brown crystals; grayish-green crystals were found to show a novel lithium–iron–copper phosphate phase,[14] while the structure of the blue-green crystals is still being determined.

Structure and Composition. Single crystal X-ray examination of the brown crystals, further called *o*-LiFeCuPhosphate, confirmed that the solid crystallizes as olivine phase, space group *Pnma*, with unit cell dimensions a = 10.226(2) Å, b = 6.012(1) Å, c = 4.682(1) Å, and V = 287.8(1) $Å^3$ (Table 1). The structure is very similar to the known $LiFePO_4$ matrix, but with slightly shorter M-O bond lengths, except for two equatorial M-O (M = Fe, Cu) bonds that get longer in the substituted compound resulting in a bit more distorted in MO_6 octahedra. Distorted MO_6 octahedra sharing corners with each other form a sheet on the *bc* plane. These sheets are stitched together via PO_4 groups lying along [100] (Figure 2a). Each of MO_6 unit is surrounded by four phosphate and six lithium ions (Figure 2b). Each Li ion located in the olivine tunnels is surrounded by four PO_4 tetrahedra and six MO_6 octahedra

dx.doi.org/10.1021/cm2026619 | *Chem. Mater.* 2012, 24, 166–173

Table 1. Crystallographic Data for the *o*-LiFeCuPhosphate

formula	$Li_{0.95}[(Fe^{2+})_{0.70}(Fe^{3+})_{0.10}Cu_{0.15}Li_{0.05})]PO_4$
formula weight	156.112
temperature	298
crystal system	orthorhombic
space group	*Pnma*
a/Å	10.226(2)
b/Å	6.0121(14)
c/Å	4.6820(11)
α/deg	90
β/deg	90
γ/deg	90
V/Å^3	287.85(11)
Z	4
ρ_{calc}/g cm^{-3}	3.603
μ/mm^{-1}	5.713
R_1,wR_2 [$I > 2\sigma(I)$]	0.0229, 0.0598
R_1,wR_2 all	0.0231, 0.0599

(Figure 2c). In comparison to the $LiFePO_4$ unit cell parameter (a = 10.337 Å, b = 6.011 Å, and c = 4.695 Å), *o*-LiFeCuPhosphate unit cell has smaller axes and volume (Table 1) which further supports the substitution.[3]

Structural refinement indicates partial occupancy on both the M1 and M2 sites corresponding to a composition of $Li_{0.95}M_{0.95}PO_4$. EDS analysis gives an Fe:Cu:P ratio of 0.75(5):0.17(3):1 confirming that the transition metals do not fully occupy the M2 site. The remaining M2 positions may be either vacant or occupied by lithium ions. The R-factor for the structural refinement becomes slightly lower when Li is placed at the M2 site, with the lowest R-factor achieved for the $Li_{0.95}[(Fe^{2+})_{0.70}(Fe^{3+})_{0.10}Cu_{0.15}Li_{0.05})]PO_4$ composition, which is consistent with the EDS results. To provide more evidence of Li occupying M2 site, we compared the unit cell volume with the value expected for the average ionic radii of the ions at the M2 site using the trend established in our previous work.[3] The linear dependence found between the cubic root of the cell volume and the ionic radius of M2 species (Figure 16 in ref 3) gives a cell volume of 288.5 Å^3 for the average radius of 0.76 Å for the 0.7 Fe^{2+}, 0.1 Fe^{3+}, 0.15 Cu^{2+}, and 0.05 Li^+. This is in good agreement with the observed 287.8 Å^3 suggesting that Li^+ is present at the M2 site. This composition is consistent with the NMR and magnetic studies as will be discussed later.

Magnetic Properties. The magnetic properties have been studied with the primary goal of determining the oxidation states of iron and copper, and also to examine the effect of copper substitution and lithium disorder on the magnetic interactions in the olivine structure. The temperature dependences of the magnetic susceptibility (Figure 3) reveal a strong anisotropy of the magnetic properties. The average magnetic susceptibility shows an antiferromagnetic transition at 48 K, somewhat lower than the 51 K observed in $LiFePO_4$. The sharp drop of the magnetic susceptibility measured in the magnetic

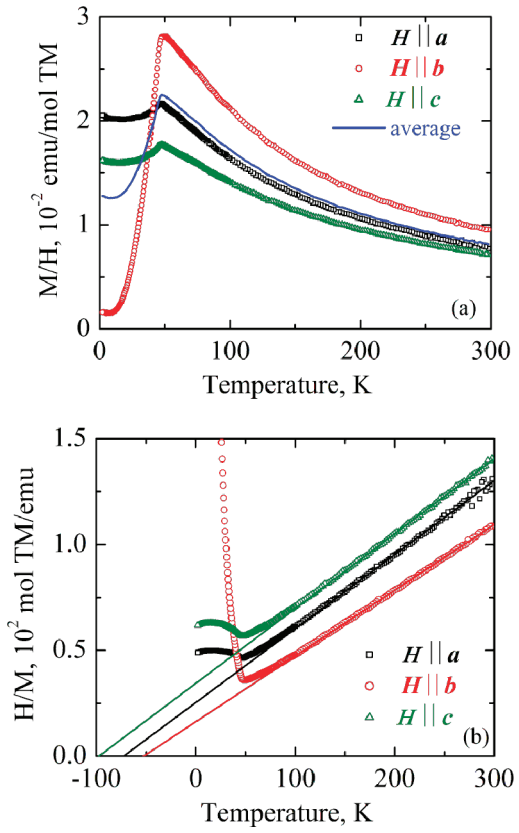

Figure 3. (a) Temperature dependences of the magnetic susceptibility of *o*-LiFeCuPhosphate measured with magnetic field applied parallel to the crystallographic axes *a*, *b*, and *c*, and their average. (b) Reciprocal susceptibilities and their fit to the Curie–Weiss law.

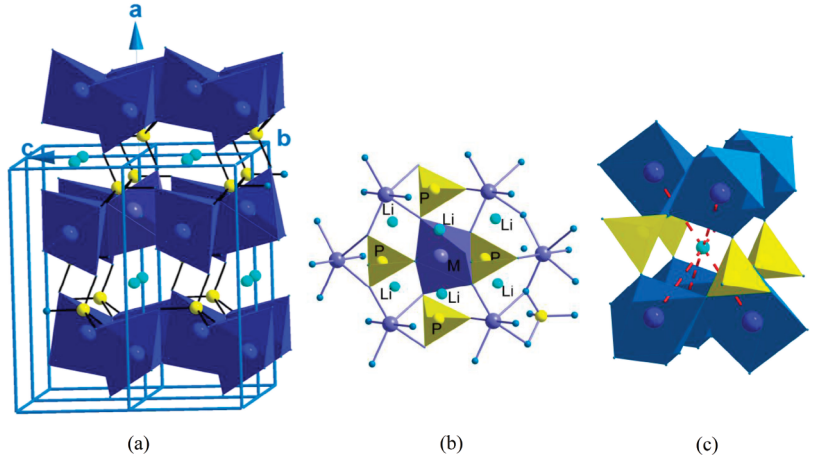

Figure 2. Olivine structure (a) viewed along *b* axis and local environments at (b) transition metal M2 and (c) lithium M1 sites.

dx.doi.org/10.1021/cm2026619 | *Chem. Mater.* 2012, 24, 166–173

field applied along the *b* crystallographic direction indicates that the spins are aligned along *b* axis in the antiferromagnetic state, similar to that in $LiFePO_4$. Above the Neel temperature the anisotropic behavior is preserved because of anisotropy of the g-factors. The temperature dependences of the magnetic susceptibility were fitted to the Curie–Weiss law $\chi_\alpha = \chi_{0,\alpha} + C_\alpha/(T - \Theta_a)$, where α is either *a*, *b*, or *c* for the susceptibility measured along *a*, *b*, and *c* crystallographic axes, respectively. All the susceptibilities were normalized per mole of the transition metals, and the effective magnetic moments were calculated using $\mu_{eff,\alpha} = (8C_\alpha)^{1/2}$. The highest effective magnetic moment is found along the *b* axis, combined with the highest value of the temperature-independent susceptibility $\chi_{0,b}$ and the weakest magnetic exchange as follows from the lowest absolute value of the Curie–Weiss constant Θ_B (Table 2). The effective

Table 2. Magnetic Properties of the *o*-LiFeCuPhosphate

orientation	T_N, K	χ_0, 10^{-4} emu/mol TM	*C*, emu K/mol TM	Θ, K	μ, μ_B
$H \parallel a$	47.5(5)	1.0	2.860(9)	−72.5(6)	4.78
$H \parallel b$	49.2(5)	3.6	3.221(8)	−52.5(4)	5.08
$H \parallel c$	47.5(5)	0.3	2.830(9)	−97.5(4)	4.76
average	48.1(5)	1.6	2.973(9)	−74.2(5)	4.88

magnetic moments measured along *a* and *c* axes are quite close to each other, with $\mu_{eff,a}$ a bit larger than $\mu_{eff,c}$. The strongest magnetic exchange is found along the *c* axis. The origin of the magnetic anisotropy lies in the electronic structure of the Fe^{2+} ion where spin–orbit coupling has to be taken into account. The theory of the anisotropic magnetic susceptibility of $LiFePO_4$ was developed by Liang et al.[23] and applied to the single crystal magnetic susceptibility. Our experimental data is consistent with this theory and shows trends similar to that of the $LiFePO_4$ single crystal. However, copper and lithium substitution leads to lower effective magnetic moments, weaker magnetic exchange, and lower T_N compared to $LiFePO_4$. T_N is expected to decrease because Fe^{2+}–Fe^{2+} magnetic exchange weakens when Fe^{2+} ($S = 2$) is substituted with Cu^{2+} ($S = 1/2$) or nonmagnetic Li^+ ions. However, Fe^{3+}–Fe^{2+} magnetic exchange is expected to be stronger than Fe^{2+}–Fe^{2+} because of higher magnetic moment of Fe^{3+} ($S = 5/2$) and shorter Fe^{3+}-O bond length. The combined contributions of Cu^{2+}, Li^+, and Fe^{3+} result in slight weakening of the magnetic exchange and the decrease of the Neel temperature. The average effective magnetic moment of 4.88 μ_B per mole of transition metals is lower than 4.9–5.4 μ_B values reported for $LiFePO_4$.[24] This experimental value is in a very good agreement with 4.92 μ_B expected for $Li_{0.95}[(Fe^{2+})_{0.70}(Fe^{3+})_{0.10}Cu_{0.15}Li_{0.05})]PO_4$ assuming the magnetic moment of Fe^{2+} to be 5.20 μ_B, the experimental result obtained for $LiFePO_4$ single crystal[23] and hydrothermally synthesized $LiFePO_4$;[24] 1.9 μ_B per Cu^{2+} (d^1, $S = 1/2$, $g = 2.2$) and the spin-only 5.92 μ_B per Fe^{3+}. If there were no lithium at the transition metal site, the fraction of Fe^{3+} ions would have been increased to 0.15 leading to an effective magnetic moment of 4.96 μ_B per mole of TM. The departure of the Fe^{2+} and Cu^{2+} magnetic moments from spin-only values is due to the orbital contribution well-known for Fe^{2+} and Cu^{2+} compounds.[25] The idea of a magnetic polaron was also put forward to explain the large effective magnetic moment in Li-deficient $LiFePO_4$.[26] The existence of a polaron is consistent with the vacancies at the Li site found by the X-ray diffraction and with the optical properties to be discussed below. However, the magnetic moment of such a polaron can hardly be estimated using a straightforward approach accepted in ref 26.

^{6}Li Solid State MAS NMR. Information on the local structure of *o*-LiFeCuPhosphate was obtained from ^{6}Li MAS NMR data. Each nonequivalent lithium site is expected to generate a distinct resonance, accompanied by spinning sidebands. Therefore, this technique is useful to ascertain the level of cation mixing in the compound. In compounds containing paramagnetic ions such as Fe^{2+} or Fe^{3+}, the shift of the resonances are dominated by through-bond Fermi contact interactions between the lithium ions and the paramagnets, through the anions, whereas the sidebands arise from the partial averaging by MAS of the large dipolar interaction between the Li nuclei and the magnetic moments of the paramagnetic centers.[27]

At first glance, the ^{6}Li MAS NMR spectrum (Figure 4) of *o*-LiFeCuPhosphate shows a single broad resonance, which

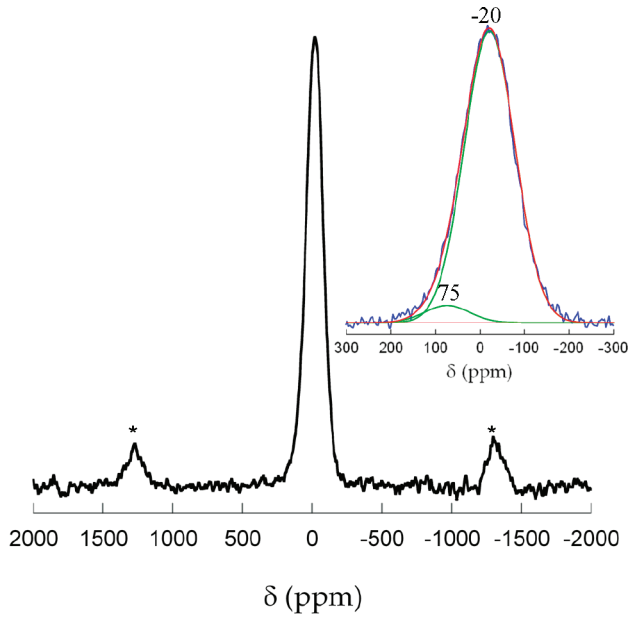

Figure 4. ^{6}Li MAS NMR spectra of orthorhombic *o*-LiFeCuPhosphate powder, acquired at 38 kHz. The spinning side bands are marked with asterisks. Inset: deconvolution (individual peaks in green, summation in red) of the signals in the isotropic region. Relevant shift values are indicated.

would be consistent with the existence of a single environment at −20 ppm. In the ideal olivine structure of $LiFePO_4$, the octahedral lithium site, M1, is coordinated by six oxygen ions connected to six iron ions in M2 sites such that there are four about 90° Li–O–Fe contacts and two of each 111 and 121.5° Li–O–Fe contacts (Figure 2).[28] The shift at which this resonance appears has been shown to greatly depend on the synthetic history of the $LiFePO_4$ sample, with signals systematically appearing at negative values, from −8 to −56 ppm.[29] Therefore, the NMR shift of −20 ppm observed here is within the range reported in the literature. The value is consistent with the fact that in the copper-doped crystals the Li–O–Fe angles differ by no more than 1° and Li–O and Fe–O bond lengths differ by no more than 0.03 Å from the respective angles and lengths of $LiFePO_4$, and is an indication that the Li interactions in this site are dominated by the majority presence of Fe^{2+} in the M2 site, with less sizable contributions of Cu^{2+} and Fe^{3+} ions. The presence of a single

dx.doi.org/10.1021/cm2026619 | *Chem. Mater.* 2012, 24, 166–173

peak with width comparable to that of pure $LiFePO_4$[30−33] indicates that all lithium ions in the M1 site are surrounded by the very close proportions of transition metal ions (in M2 sites), other lithium ions (both in M1 and M2) and vacancies (in M1). Hence, the data point at the existence of local ordering in the compound through the formation of cation clusters.

Close inspection of the main ^6Li resonance reveals the existence of a slight asymmetry at positive shifts. Additional information on this was obtained by spectral deconvolution; a good fit was obtained by adding a single, small peak at about 75 ppm (Figure 4). It must be noted that the close proximity with the major signal and the weak intensity of this shoulder makes it difficult to accurately determine its position and intensity, and, hence, results in errors that make this information only partially quantitative. Similar minor peaks have been observed in defective $LiFePO_4$ samples with Li ions in the M2 site and small amounts of Fe^{3+} in both cationic sites,[32] and Li resonances at positive shifts are typical of Fe^{3+} phosphate phases.[34−37] Therefore, the resonance is the fingerprint of the existence of a small amount of Li ions in M2 sites, which are surrounded by Fe^{3+}. Since the NMR intensities are proportional to the amount of ions in each site, an estimation of the content of Li in M2 can be made from the deconvolution results; the resulting value, about 5% of the total Li, is consistent with the composition based on the single crystal refinements. Since no evidence was found of the presence of Fe^{3+} ions in the M1 site and their concentration in M2 is very small, a hypothesis is proposed that, in order to produce such a positive NMR shift, they must necessarily cluster around the Li^+. This type of clustering is not unprecedented and would be energetically beneficial because of the introduction of charge balance in the M2 site.

Optical Properties. Our interest in the optical properties of this copper-doped material was motivated by its rich dark-brown color and by scarcity of the experimental data pertaining to the electronic structure and vibrational properties of doped olivines. The inset of Figure 5 displays the spectrum of the

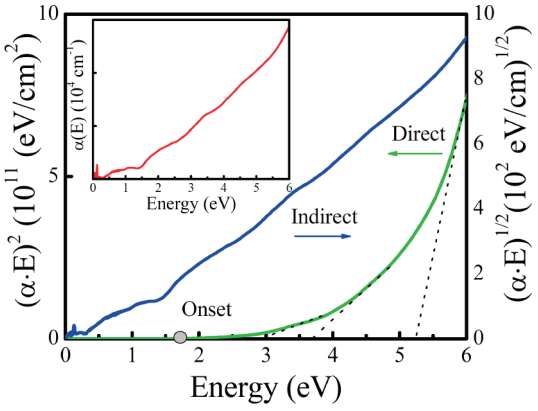

Figure 5. Energy gap determination, with tests for the direct/allowed and indirect/allowed gap. The inset shows the 300 K absorption profile of the isotropic (pressed powder) sample.

polycrystalline sample. This orientational averaging combined with chemical (metal site) disorder contributes to the diffuse spectral response. The response is typical of a semiconductor, with strong phonons, a static dielectric constant $\varepsilon_1(0) = 9$, and overall low absorption. Several broad bands are observed, centered at 1, 2, 3.5, and 4.5 eV. There is no strong absorption band in the 1−1.5 eV region as would be expected for metal to metal charge transfer. We therefore assign the observed excitations as d to d and p to d in nature. The diffuse character of the optical response is related to the polycrystalline nature of this sample which averages the directional response and the substantial replacement of iron centers with copper, a substitution that works to fill up the gap with new states. Modest conductivity from small polarons is present in the near-infrared with an ∼0.3 eV onset and center at E_{pol} ∼1 eV. As a consequence of large U and polaronic picture, the bands are flat with a large effective mass. Within the polaron picture and simple hoping model, $E_a = E_{pol}/4$, which gives the activation energy E_a = 1 eV/4 = 0.25 eV, in agreement with transport studies. The onset for optical conductivity is observed at ∼1.65 eV, although absorption is low, consistent with weak p−d hybridization. The band gap analysis is presented in the main panel of Figure 5. It indicates a direct band gap of ∼3.6 eV, in excellent agreement with electronic structure calculations that predict a 3.7 eV minority channel gap between d states for U = 4.7.[38] The charge gap corresponding to oxygen p to transition metal d excitations is observed near 5.2 eV.

The infrared response was measured on both an isotropic sample and on the bc plane of an indexed single crystal (Figure 6).

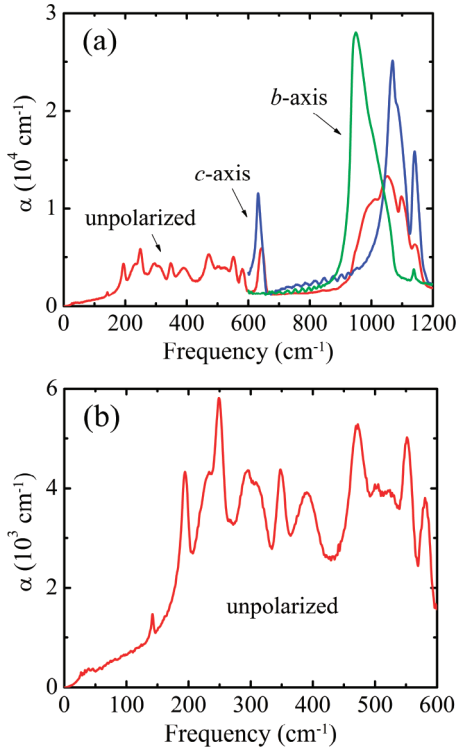

Figure 6. (a) 300 K infrared absorption spectrum of *o*-LiFeCuPhosphate isotropic sample (red line) and single crystal along [010] (green) and [001] (blue). (b) Close-up view of the far-infrared spectrum.

The vibrational features of Li_xFePO_4 and related compounds are traditionally assigned based upon an analysis of local structure and a functional group approach. This approach can be useful, but it is important to realize that vibrational modes in this material are actually very collective. This is especially true for the low frequency modes, which have complicated displacement patterns involving many centers and should be regarded as phonons. The main consequence of Cu insertion is band broadening with respect to pristine $LiFePO_4$. Stretching

dx.doi.org/10.1021/cm2026619 | *Chem. Mater.* 2012, 24, 166−173

PO_4^{3-} modes are observed between 900 and 1200 cm^{-1}. The 633 cm^{-1} peak is traditionally assigned as a FeO_6 stretching mode and will be discussed in more detail below. Bending and combination modes of the oxo-anions appear between 400 and 600 cm^{-1}. The lower frequency far-infrared features involve complex motion of the PO_4^{3-} building blocks relative to transition metal centers; they are related to the Fe valence state. The 386, 348, and 249 cm^{-1} modes in Li_xFePO_4 are relatively unchanged in our material (389, 348, and 249 cm^{-1}). The 249 cm^{-1} mode appears with enhanced oscillator strength compared with the parent compound. The 287 cm^{-1} feature splits into a doublet centered at 294 and 313 cm^{-1}. The 196 cm^{-1} mode red shifts to 193 cm^{-1} and appears in this substituted olivine with increased intensity. The lithium motion can be accessed from the 233 cm^{-1} asymmetric cage vibration of Li in Li_xFePO_4, which appears here at 230 cm^{-1}. Our results indicate that the Li cage environment in the parent compound is similar to that in our material. A clear lattice mode is observed at 141 cm^{-1}, likely involving relative Li and Fe-related displacements.

We also measured the vibrational properties of a small single crystal in the *bc* plane (Figure 6). This data is presented in comparison with the aforementioned isotropic data. It shows strong polarization of PO_4^{3-} stretching vibrations between 900 and 1200 cm^{-1}. Moreover, the metal-oxide stretch near 633 cm^{-1} is preferentially polarized in the *c* direction. It is also much more intense in the single crystal than in the isotropic pellet data. The 633 cm^{-1} peak related to metal oxide stretching in the FeO_6 octahedra is known to be sensitive to charge and appears as a doublet in Li_xFePO_4 (636 and 647 cm^{-1}). The fact that it appears as a broad singlet with a strong shoulder in this copper-doped compound simply reflects the natural disorder in this material, which emanates from both the dual FeO_6 and CuO_6 environments and the slight (x = 0.95) lithium deficiency at the M1 site.

Electrochemical Properties. Figure 7 shows the first electrochemical cycle of *o*-LiFeCuPhosphate powder. A plateau

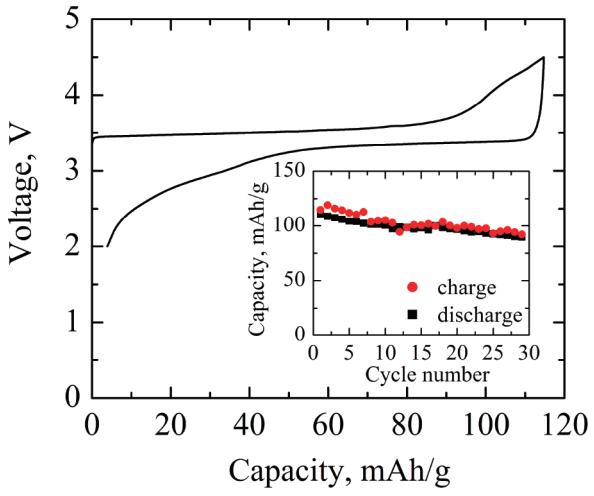

Figure 7. Galvanic cycling of *o*-LiFeCuPhosphate between 2.0 at 4.5 V at current density of 0.1 mA/cm^2. Inset: Capacity retention over first 30 cycles.

at 3.4 V, corresponding to the Fe^{2+}/Fe^{3+} redox potential, is observed, with an onset of a second process above 4 V. The inset in Figure 7 shows the capacity retention of this cell over the first several cycles. The first charge has 115 mAh/g of capacity, which is close to the "iron only" capacity of 120 mAh/g for oxidation of all the ferrous to ferric. The subsequent lithium insertion shows a capacity of 110 mAh/g, as might be expected for the normal first-cycle loss. However, in this case there are 5% vacancies on the lithium site that could be filled reducing half of 10% ferric ions present in the pristine compound. The GITT method was used to more accurately determine the capacity of the material, as it comes closer to equilibrium conditions than the cycling described above. Figure 8

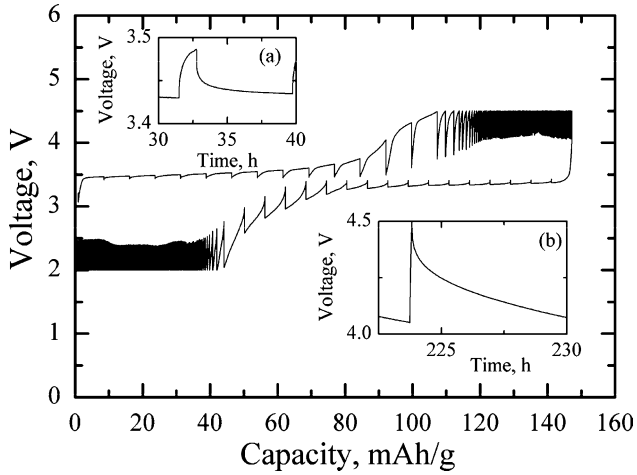

Figure 8. GITT data of *o*-LiFeCuPhosphate plotted as voltage vs capacity. Inset-*a*: capacity vs time plot of step three during iron oxidation. Inset-*b*: capacity vs time plot of step 28 during 4.1 V plateau.

shows that the capacity of the first charge approaches 140 mAh/g; however, above 115 mAh/g the capacity gained at each GITT step diminishes very quickly. Similar behavior is observed upon discharge, with about 115 mAh/g capacity obtained with reasonable GITT steps. The onset of the 4.1 V process is also observed in GITT data.

To clarify the nature of the second redox process, the impact of Cu content on the average Li intercalation voltage of $Li[Fe_{1-y}Cu_y]PO_4$ (y = 0, $^1/_4$, $^1/_2$, 1) was investigated using DFT calculations with the HSE06 hybrid functional. The voltages obtained computationally correspond to average voltages obtained for a full lithiation/delithiation. Figure 9 shows the intercalation voltage for $Li(Fe_{0.85}Cu_{0.15})PO_4$ as a function of Li content constructed using the values obtained for y = 0 and y = 1 assuming two-phase consecutive oxidation of Fe and Cu. In the absence of Cu, the voltage of 3.33 V is in reasonable agreement with experimental voltages found for $LiFePO_4$. For $LiCuPO_4$ a very high voltage of 5.44 V is obtained. According to hybrid DFT calculations, the Cu^{2+}/Cu^{3+} redox couple is therefore approximately 2 V higher than the Fe^{2+}/Fe^{3+} couple. The results obtained for $LiCuPO_4$ are similar to those recently obtained for $LiNiPO_4$.[39,40] Indeed, the Li intercalation potential of $LiNiPO_4$ was found to be significantly higher than the Li intercalation potential of the equivalent Mn, Fe, and Co phosphates. The higher intercalation potential was interpreted as stemming from the greater electronic hybridization found in the Ni−O interaction and the participation of the oxygen in the electron transfer. Similar results are found for $LiCuPO_4$ leading us to conclude that the high Cu^{2+}/Cu^{3+} redox couple is likely the consequence of a more covalent bonding between the Cu and O atoms. It should be noted that the redox potential of Cu^{2+}/Cu^{3+} in LiFeCuPhosphate is likely to be less

dx.doi.org/10.1021/cm2026619 | *Chem. Mater.* 2012, 24, 166–173

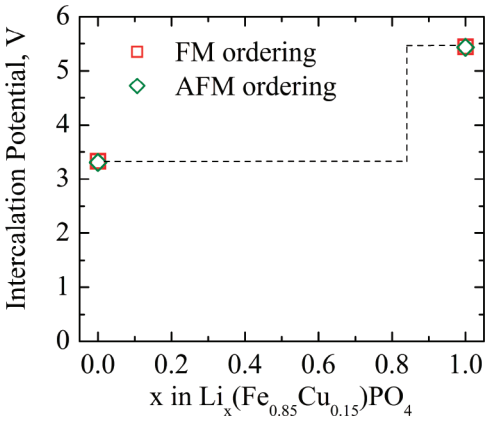

Figure 9. Intercalation potential of Li(Fe$_{0.85}$Cu$_{0.15}$)PO$_4$ reconstructed from average intercalation potential calculated for LiFePO$_4$ and LiCuPO$_4$ using DFT with the HSE06 hybrid functional. The lines are given to guide the eye.

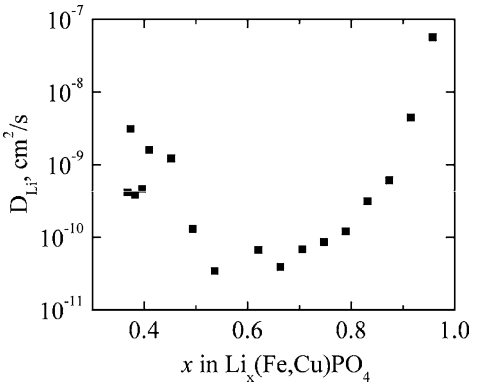

Figure 10. Lithium diffusion coefficient in *o*-LiFeCuPhosphate as a function of lithium occupancy.

than in LiCuPO$_4$. A similar effect is observed for Mn^{2+}/Mn^{3+} redox potential in LiFe$_{1-y}$Mn$_y$PO$_4$[41] and for Co^{2+}/Co^{3+} in LiMn$_{1/3}$Fe$_{1/3}$Co$_{1/3}$PO$_4$.[42] However, very little capacity is observed at each GITT step of the 4.1 V process, and its voltage is much lower than the predicted for Cu^{2+}/Cu^{3+} oxidation. Therefore we tentatively assign the voltage increase at the end of charge to the removal of Li from the iron site.[43]

The equilibrium voltage obtained from the GITT shows just a little slope upon the removal of the first 0.5Li, changed with a significantly increased slope, indicating that the Li removal might proceed as a single-phase reaction. This allows determination of the lithium diffusion coefficient via GITT, given the relaxation time is sufficient to allow the system to reach equilibrium. The seven hour relaxation time proved adequate during the lower voltage oxidation process but inadequate during the higher voltage process. This is evident from the insets in Figure 8. The steps shown in inset-*a* and inset-*b* are representative of each step during the 3.4 V and the 4.1 V plateau respectively. During the 3.4 V plateau, each $1^1/_4$ h pulse increased the cell voltage by about 0.06 V and each subsequent relaxation was sufficient to allow the voltage to descend to a near constant value, indicating equilibrium. During the higher voltage process the voltage increases by 0.45 V within the first few minutes of each pulse and subsequent relaxation was unable to reach a constant value. This indicates slower lithium diffusion during the higher voltage process. Lithium diffusion coefficients calculated from data collected during the 3.4 V plateau and an onset of high-voltage process are shown in Figure 10. These coefficients were calculated using eq 1 of Weppner and Huggins.[44]

$$D^{\mathrm{GITT}} = \frac{4}{\pi\tau}\left(\frac{m_B V_M}{M_B S}\right)^2\left(\frac{\Delta E_s}{\Delta E_t}\right)^2 \quad (1)$$

In this equation, τ is the constant current pulse time; m_B, V_M, and M_B are the mass, the molar volume, and the molar mass of the insertion electrode material, respectively. S is the area of the electrode−electrolyte interface, ΔE_s is the change of the steady-state voltage during a single-step GITT experiment, and ΔE_t is the total change of cell voltage during a constant current pulse τ of a single-step GITT experiment. The molar volume was calculated from the single crystal lattice parameters of X-ray diffraction data. The diffusion coefficient shows a flat minimum at about 10^{-10} cm^2 s^{-1} when the lithium site occupancy is between 0.8 and 0.5, while at higher and lower Li content, the diffusion coefficient is higher. It decreases fast from 5.7×10^{-8} cm^2 s^{-1} for Li$_{0.9}$[Fe$_{0.80}$Cu$_{0.15}$Li$_{0.05}$]PO$_4$ to the above-mentioned minimum value at the beginning of charge, and then increases again to 5×10^{-9} cm^2 s^{-1} when less than 0.4Li remains in the structure. If the delithiation process proceeded as a single-phase reaction, the diffusion coefficient would increase as more vacancies become available upon delithiation. The observed minimum might indicate a two-phase reaction, as in bulk LiFePO$_4$, at least over the Li$_{0.8}$−Li$_{0.5}$ range upon charge. The minimum can then be explained by the accumulation of accommodation energy generated by the lattice mismatch due to the different molar volumes of the lithium rich and the lithium dilute phase.[45] The accommodation energy will slow down phase migration and will be maximized when the contact area between the lithium rich and the lithium dilute phase is greatest. The faster diffusion at higher and lower Li content suggests single-phase cycling outside of the immiscibility gap region, which is also evident from the sloping voltage profile especially pronounced toward the end of charge (Figures 7, 8). The lithium diffusion coefficient over these Li contents is close to the value predicted by Ceder et al. for LiFePO$_4$.[46]

CONCLUSIONS

Copper substituted lithium iron phosphate single crystals were formed under hydrothermal conditions when a copper reaction vessel was used. One of the phases formed has the olivine structure, with 15% copper on the iron site, and partial occupancy of both Li and transition metal sites, Li$_{0.95}$[(Fe^{2+})$_{0.70}$(Fe^{3+})$_{0.10}$-(Cu^{2+})$_{0.15}$Li$_{0.05}$)]PO$_4$. X-ray and NMR studies confirmed 5% lithium in the iron site and Fe^{3+} clustering around the lithium ions. Single crystal magnetic studies show antiferromagnetic behavior below 48 K with the magnetic moments aligned along [010]. The optical spectra show that the electronic excitations are d-d and p-d in nature, and not charge transfer. The compound delivers a discharge capacity of 110 mA h g^{-1} when cycled between 2 and 4.5 V at a current density of 0.1 mA cm^{-2}. Two redox processes, one at 3.4 V corresponding to Fe^{2+}/Fe^{3+}, and the other at 4.1 V are observed. The redox potential of Cu^{2+}/Cu^{3+} is found to be above 5 V from the DFT calculation, which is significantly higher than the experimentally observed 4.1 V, indicating that Cu is probably not redox active under the experimental conditions used in this study. The higher voltage redox process might also be associated with Li removal from the transition metal site, ion clustering, or a side reaction.

dx.doi.org/10.1021/cm2026619 | *Chem. Mater.* 2012, 24, 166−173

GITT data indicates that 3.4 V charge process is likely to be a two-phase reaction, since the equilibrium voltage is nearly constant up to about $Li_{0.5}Fe_{0.8}Cu_{0.15}PO_4$, composition. Further Li removal appears to be single-phase as reaction voltage steadily increases. The diffusion coefficient determined over this region increases from 10^{-10} to 5×10^{-9} cm^2 s^{-1} as more Li is being removed.

AUTHOR INFORMATION

Corresponding Author

*E-mail: stanwhit@gmail.com.

Present Addresses

▲Primet Precision, 950 Danbury Road, Ithaca, NY 14850

⊗Pacific Northwest National Laboratory, 902 Battelle Blvd, Richland, WA.

▼Chemistry Department, Broome Community College, Binghamton, NY 13901

○Environmental Energy Technologies Division, Lawrence Berkeley National Laboratory, Berkeley, CA 94720.

#Department of Chemistry, Cambridge University, Cambridge, U.K.

▽3M, St. Paul, MN 55144.

Author Contributions

The manuscript was written through contributions of all authors.

ACKNOWLEDGMENTS

The work at Binghamton, MIT, and Stony Brook is supported as part of the Northeastern Center for Chemical Energy Storage, NECCES, an Energy Frontier Research Center funded by the U.S. Department of Energy, Office of Science, and Office of Basic Energy Sciences under Award Number DE-SC0001294. The Binghamton group also acknowledges financial support from the National Science Foundation, DMR 0705657 for partial support of the magnetic measurements, and for the purchase of the magnetometer. J.C. is indebted to Generalitat de Catalunya for funding through a Beatriu de Pinós fellowship.

REFERENCES

(1) Padhi, A. K.; Nanjundaswamy, K. S.; Goodenough, J. B. *J. Electrochem. Soc.* **1997**, *144*, 1188.

(2) Yang, S.; Zavalij, P. Y.; Whittingham, M. S. *Electrochem. Commun.* **2001**, *3*, 505.

(3) Chen, J.; Vacchio, M. J.; Wang, S.; Chernova, N.; Zavalij, P. Y.; Whittingham, M. S. *Solid State Ionics* **2008**, *178*, 1676.

(4) Meethong, N.; Huang, H.-Y. S.; Carter, W. C.; Chiang, Y.-M. *Electrochem. Solid-State Lett.* **2007**, *10*, A134.

(5) Meethong, N.; Huang, H.-Y. S.; Speakman, S. A.; Carter, W. C.; Chiang, Y.-M. *Adv. Funct. Mater.* **2007**, *17*, 1115.

(6) Hong, J.; Wang, C. S.; Kasavajjula, U. *J. Power Sources* **2006**, *162*, 1289.

(7) Hong, J.; Wang, C. S.; Chen, X.; Upreti, S.; Whittingham, M. S. *Electrochem. Solid-State Lett.* **2009**, *12*, A33.

(8) Wang, D.; Ouyang, C.; Drézen, T.; Exnar, I.; Kay, A.; Kwon, N.-H.; Gouerec, P.; Miners, J. H.; Wang, M.; Grätzel, M. *J. Electrochem. Soc.* **2010**, *157*, A225.

(9) Chung, S.-Y.; Bloking, J. T.; Chiang, Y.-M. *Nat. Mater.* **2002**, *1*, 123.

(10) Herle, P. S.; Ellis, B.; Coombs, N.; Nazar, L. F. *Nat. Mater.* **2004**, *3*, 147.

(11) Ellis, B.; Herle, P. S.; Rho, Y.-H.; Nazar, L. F.; Dunlap, R.; Perry, L. K.; Ryan, D. H. *Faraday Discuss.* **2007**, *134*, 119.

(12) Chen, J.; Whittingham, M. S. *Electrochem. Commun.* **2006**, *8*, 855.

(13) Yang, S.; Song, Y.; Zavalij, P. Y.; Whittingham, M. S. *Electrochem. Commun.* **2002**, *4*, 239.

(14) Upreti, S.; Yakubovich, O. V.; Chernova, N. A.; Whittingham, M. S. *Acta Crystallogr., Sect. E* **2011**, *67*, i29.

(15) *SMART, Bruker Molecular Analysis Research Tool*, Version 5.0 618; Bruker AXS Inc.: Madision, WI, 2000.

(16) *SAINT-NT and SHELXTL-NT*; Bruker AXS Inc.: Madision, WI, 2001.

(17) Sheldrick, G. M. *Acta Crystallogr., Sect. A* **1990**, *46*, 467.

(18) Pankove, J. I. *Optical processes in semiconductors*; Courier Dover Publications: Mineola, NY, 1971.

(19) Heyd, J.; Scuseria, G. E.; Ernzerhof, M. *J. Chem. Phys.* **2003**, *118*, 8207.

(20) Paier, J.; Marsman, M.; Hummer, K.; Kresse, G.; Gerber, I. C.; Angyan, J. G. *J. Chem. Phys.* **2006**, *125*, 249901.

(21) Heyd, J.; Scuseria, G. E.; Ernzerhof, M. *J. Chem. Phys.* **2006**, *124*, 219906.

(22) Aydinol, M. K.; Kohan, A. F.; Ceder, G.; Cho, K.; Joannopoulos, J. D. *Phys. Rev. B* **1997**, *56*, 1354.

(23) Liang, G.; Park, K.; Li, J.; Benson, R. E.; Vaknin, D.; Markert, J. T.; Croft, M. C. *Phys. Rev. B* **2008**, *77*, 064414.

(24) Chernova, N. A.; Nolis, G. M.; Omenya, F. O.; Zhou, H.; Li, Z.; Whittingham, M. S. *J. Mater. Chem.* **2011**, *21*, 9865.

(25) Mabbs, F. E.; Machin, D. J. *Magnetism and Transition Metal Complexes*; Chapman and Hall: London, U.K., 1973.

(26) Zaghib, K.; Mauger, A.; Goodenough, J. B.; Gendron, F.; Julien, C. M. *Chem. Mater.* **2007**, *19*, 3740.

(27) Grey, C. P.; Dupré, N. *Chem. Rev.* **2004**, *104*, 4493.

(28) Santoro, R. P.; Newnham, R. E. *Acta Crystallogr.* **1967**, *22*, 344.

(29) Cabana, J.; Grey, C. P. In *Energy Production and Storage: Inorganic Chemical Strategies for a Warming World*; Crabtree, R. H., Ed.; John Wiley & Sons: West Sussex, U.K., 2010; p 375.

(30) Tucker, M. C.; Doeff, M. M.; Richardson, T. J.; Fiñones, R.; Cairns, E. J.; Reimer, J. A. *J. Am. Chem. Soc.* **2002**, *124*, 3832.

(31) Recham, N.; Casas-Cabanas, M.; Cabana, J.; Grey, C. P.; Jumas, J. C.; Dupont, L.; Armand, M.; Tarascon, J. M. *Chem. Mater.* **2008**, *20*, 6798.

(32) Hamelet, S.; Gibot, P.; Casas-Cabanas, M.; Bonnin, D.; Grey, C. P.; Cabana, J.; Leriche, J.-B.; Rodriguez-Carvajal, J.; Courty, M.; Levasseur, S.; Carlach, P.; Van Thournout, M.; Tarascon, J. M.; Masquelier, C. *J. Mater. Chem.* **2009**, *19*, 3979.

(33) Cabana, J.; Shirakawa, J.; Chen, G.; Richardson, T. J.; Grey, C. P. *Chem. Mater.* **2010**, *22*, 1249.

(34) Davis, L. J. M.; Heinmaa, I.; Goward, G. R. *Chem. Mater.* **2010**, *22*, 769.

(35) Castets, A.; Carlier, D.; Trad, K.; Delmas, C.; Menetrier, M. *J. Phys. Chem. C* **2010**, *114*, 19141.

(36) Kim, J.; Middlemiss, D. S.; Zhu, B. Y. X.; Chernova, N. A.; Masquelier, C.; Grey, C. P. *J. Am. Chem. Soc.* **2010**, *132*, 16825.

(37) Shirakawa, J.; Cabana, J.; Wakihara, M.; Grey, C. P. *J. Mater. Chem.* **2011**, *21*, 10012.

(38) Zhou, F.; Kang, K.; Maxisch, T.; Ceder, G.; Morgan, D. *Solid State Commun.* **2004**, *132*, 181.

(39) Chevrier, V. L.; Ong, S. P.; Armiento, R.; Chan, M. K. Y.; Ceder, G. *Phys. Rev. B* **2010**, *82*, 075122.

(40) Zhou, F.; Cococcioni, M.; Kang, K.; Ceder, G. *Electrochem. Commun.* **2004**, *6*, 1144.

(41) Kobayashi, G.; Yamada, A.; Nishimura, S.; Kanno, R.; Kobayashi, Y.; Seki, S.; Ohno, Y.; Miyashiro, H. *J. Power Sources* **2009**, *189*, 397.

(42) Gwon, H.; Seo, D.-H.; Kim, S.-W.; Kim, J.; Kang, K. *Adv. Funct. Mater.* **2009**, *19* (20), 3285.

(43) Seo, D.-H.; Gwon, H.; Kim, S.-W.; Kim, J.; Kang, K. *Chem. Mater.* **2010**, *22*, 518.

(44) Weppner, W.; Huggins, R. A. *J. Electrochem. Soc.* **1977**, *124*, 1569.

(45) Zhu, Y.; Wang, C. *J. Phys. Chem. C* **2010**, *114*, 2830.

(46) Morgan, D.; Van der Ven, A.; Ceder, G. *Electrochem. Solid-State Lett.* **2004**, *7*, A30.